Theoretical Equation of State of Dense Nonconformal Fluids from Effective Potentials. 1. Applications to Model Systems

ARTICLE *in* THE JOURNAL OF PHYSICAL CHEMISTRY B · AUGUST 2001

Impact Factor: 3.3 · DOI: 10.1021/jp011321f

2 AUTHORS:

Orlando Guzmán
Metropolitan Autonomous University
40 PUBLICATIONS **413** CITATIONS

SEE PROFILE

Fernando Del Río
Universidad Autónoma Metropolitana, Mexic…
91 PUBLICATIONS **917** CITATIONS

SEE PROFILE

Theoretical Equation of State of Dense Nonconformal Fluids from Effective Potentials. 1. Applications to Model Systems

Orlando Guzmán and Fernando del Río*

Universidad Autónoma Metropolitana, Iztapalapa, Apdo 55 534, México DF, 09340 México

Received: April 10, 2001

The approximate nonconformal (ANC) theory, successfully applied to dilute gases, is generalized to dense fluids. Monte Carlo simulations were performed for several ANC potentials, used as effective nonconformal interactions in the theory. These results were used to assess the performance of alternate equations of state (EOS). Perturbation theory illuminates the effects of nonconformality but fails to produce an EOS of ANC fluids of the needed accuracy. An accurate empirical EOS was found for supercritical fluids and used to test the applicability of the theory. EOSs were found for Lennard-Jones, two-center Lennard-Jones, linear Kihara, and square well heterodiatiomic fluids. These theoretical EOSs are in good agreement with simulation results of the same fluids. The effective potentials of the nonspherical systems are found to be state-dependent with parameters modeled by a low order virial-like series. These results give a basis for the application of the theory to real dense fluids.

1. Introduction

The principle of corresponding states (PCS), introduced by J. D. van der Waals in 1880, is valid for two or more fluids with potentials of the same form but different scale parameters (say ϵ, the depth of the minimum of potential, and r_m, the position of this minimum). This principle says that the thermodynamic properties of these fluids are equal when they are written in units of the ϵ and r_m of each fluid. The potential functions of fluids satisfying the PCS are said to be "conformal".[1] In particular, the reduced equation of state (EOS) is the same for a set of conformal fluids, such as, to very good approximation, the noble gases Ar, Kr, and Xe. However, this principle states an "all or nothing" relationship between the potentials and has little to say about the EOS of fluids with nonconformal potentials. Because of this limitation, several extensions to the PCS have been proposed but these have been mainly empirical. A good example is Pitzer's theory for gases, which introduces the acentric factor as a new parameter which allows to construct the EOS of nonconformal gases.[2] Despite their practical use, empirical extension to the PCS are unsatisfactory from the statistical mechanical approach because the shape parameters such as the acentric factor are not related directly to the molecular features of the fluids.

Recently, the approximate nonconformal (ANC) theory was proposed as a rigorous extension of the PCS for gases.[3] It introduces the softness of the potential, *s*, as a new molecular parameter accounting for the form of the potential profile. The ANC theory uses an effective spherical potential depending on ϵ, r_m, and *s*, which has allowed us to account for the second virial coefficient $B(T)$ of a wide class of nonconformal substances and their binary mixtures. Given the theoretical and practical interest of dense fluids, it is desirable to test the applicability of the ANC theory in liquids. That such an extension is feasible is supported by the correlations exhibited between the softness *s* and the critical constants of more than 50 real substances.[4] Thus, we conjecture here that the notion of softness of the potential is relevant also at liquidlike densities.

In the present paper, we extend the ANC theory to dense fluids and apply it to construct the EOS of several systems of interest. Because of the influence of many-body forces on properties of real substances, at this stage, we test the ANC theory on model fluids with strictly binary interactions, reserving its application to real substances for future work.

The rest of the paper is organized as follows: In section 2, we review the ANC theory, defining the ANC family of nonconformal potentials and giving a precise definition of the softness, *s*. The usefulness of the concept of effective potentials in dense fluids is also discussed. In section 3, we describe the MC simulations used to calculate *pVT* surfaces for several ANC systems, which are then used in section 4 to assess the performance of common routes in the theory of liquids to the ANC EOS. In section 5, we discuss the applicability of ANC potentials as effective interactions for model fluids and exemplify the behavior of the effective parameters (ϵ,r_m, and *s*) by applying the ANC theory to four model potentials, both spherical and nonspherical. Conclusions are given in section 6.

2. ANC Theory

2.1. ANC Potentials for Gases. For density (ρ), temperature (T), pressure (p), and the second virial coefficient (B), we use the reduced variables $\rho^* = \rho r_m^3$, $T^* = kT/\epsilon = 1/\beta\epsilon$, $p^* = pr_m^3/\epsilon$, and $B^* = B/(2\pi r_m^3/3)$, respectively.

The ANC theory for gases was introduced to understand why the virial coefficients $B_x^*(T^*)$ and $B_y^*(T^*)$ of many substances *x* and *y* are related linearly as[3]

$$B_x^*(T^*) = c_0 + c_1 B_y^*(T^*) \tag{1}$$

where c_0 and c_1 are parameters that depend on the nonconformality between *x* and *y*. If the substances are conformal, $c_0 = 0$ and $c_1 = 1$ obtaining the PCS relation: $B_x^*(T^*) = B_y^*(T^*)$. For many real substances, eq 1 holds to a very good approximation

* To whom correspondence should be addressed. E-mail: fdr@xanum.uam.mx.

10.1021/jp011321f CCC: $20.00
Published on Web 08/07/2001

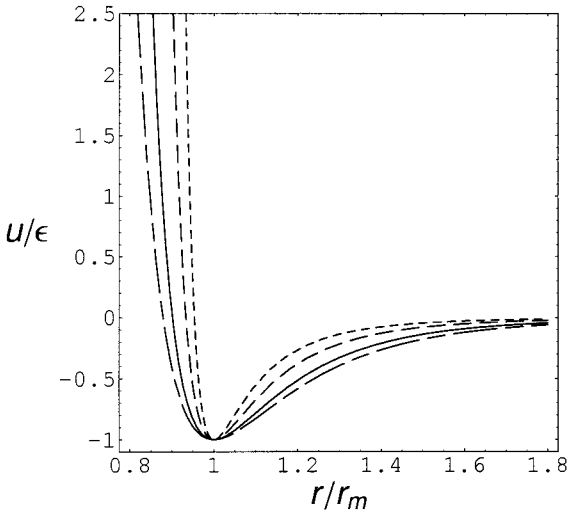

Figure 1. ANC reference potential (solid line) and examples with different softness $s = 0.5$, 0.7, and 1.2 (dotted, short−short dashed, and long−short dashed lines, respectively).

and c_0 and c_1 depend only on the form parameters s_x and s_y. To explain the linear relation above, the ANC theory introduces a family of potentials whose form changes continuously with s from that of a reference system. The reduced reference potential, u_1^*, is chosen as a Kihara function

$$u_1^*(z) = \left(\frac{1-a_0}{z-a_0}\right)^{12} - 2\left(\frac{1-a_0}{z-a_0}\right)^{6} \tag{2}$$

where $z = r/r_m$ and the constant $a_0 = 0.095\,738\,911\,61$ is chosen to reproduce the experimental $B(T)$ data for argon.[3] The desired ANC family of potentials is obtained from eq 2 by substituting z by $\zeta = (1 + (z^3 - 1)/s)^{1/3}$ to get

$$u_s^*(z) = \left(\frac{1-a}{\zeta(z;s)-a}\right)^{12} - 2\left(\frac{1-a}{\zeta(z;s)-a}\right)^{6} \tag{3}$$

Of course, by setting $s = 1$ in eq 3, we recover $u_1^*(z)$. The effect of changing s can be assessed from Figure 1 that shows that the steepness of the ANC potential grows as s goes to zero. This suggests calling s the softness of the potential.

A precise definition of s for any spherical potential $u^*(z;\alpha)$, where $\alpha = \{\alpha_1, \alpha_2, ...\}$ is a set of shape parameters, is found by first inverting the relation $\phi = u^*(z;\alpha) + 1$, separately in the attractive and repulsive branches of the potential, to obtain the function $z^3(\phi,\alpha)$ and then calculating its derivative

$$\kappa_\phi([u^*]) = \frac{\partial z^3}{\partial \phi}$$

The softness s of $u^*(z;\alpha)$ with respect to reference $u_1^*(z)$ is then defined as the average

$$s = \left\langle \frac{\kappa_\phi([u^*])}{\kappa_\phi([u_1^*])} \right\rangle_\phi \tag{4}$$

In general, this process leads to different values of s for the attractive and repulsive parts of the interaction. A first-order approximation in the ANC theory, shown to be sufficient to account for $B(T)$ within experimental error, assumes the equality of these two values of s. Here we consider only this one-s approximation.[3]

The ANC family $u_s(r)$ follows eq 1 exactly. Moreover, the virial coefficient $B_s^*(T^*)$ for an ANC potential of softness s can be written in terms of repulsive and attractive volumes b^* and Λ^*

$$B_s^*(T^*) = e^{\beta\epsilon} b_s^*(T^*) - (e^{\beta\epsilon} - 1)\Lambda^*_s(T^*) \tag{5}$$

where both b_s^* and Λ_s^* obey relations similar to those in eq 1

$$b_s^*(T^*) = 1 - s + s b_1^*(T^*) \tag{6}$$

$$\Lambda_s^*(T^*) = 1 - s + s\Lambda_1^*(T^*) \tag{7}$$

with b_s^* and Λ_s^* defined as

$$b_s^*(T^*) = \beta\epsilon \int_0^\infty z^3(\phi,[u_s^*]) e^{-\beta\epsilon\phi}\, d\phi$$

$$\Lambda_s^*(T^*) = \frac{\beta\epsilon}{1 - e^{-\beta\epsilon}} \int_0^1 z^3(\phi,[u_s^*]) e^{-\beta\epsilon\phi}\, d\phi$$

Straightforward substitution of eqs 6 and 7 into eq 5 yields the desired linear relation between the second virial coefficients of ANC fluids:

$$B_s^*(T^*) = 1 - s + s B_1^*(T^*) \tag{8}$$

For other families of realistic, spherical potentials, eq 8 holds only as an approximation (hence the name of the theory). In these cases, the theory uses the ANC system with the calculated value of s to represent effectively the original one. This means that even if the effective ANC potential is different from the real pair potential both lead to the same $B(T)$ to a good approximation. For nonspherical potentials, eq 4 includes averaging over intermolecular orientations in calculating s (see ref 3).

In this way, the ANC theory is able to construct potentials that represent $B(T)$ for a wide variety of systems, from model potentials (e.g., Lennard-Jones, linear Kihara, n-site Lennard-Jones, homonuclear square well chains, and heteronuclear bonded square wells) to real substances and their binary mixtures (noble gases, nonpolar and slightly polar diatomics, alkanes, and perfluoroalkanes). When the true pair potential is known, as for model fluids and some simple substances, the effective potential can be calculated explicitly from averages such as eq 4. However, when the pair potential is not known accurately, the ANC parameters ϵ, r_m, and s are determined from experimental $B(T)$ data by a least-squares technique. Either way, we obtain an effective potential for a given gas that captures the simplest and most characteristic features of the interaction. We discuss next the meaning of effective potentials in dense fluids and how to obtain them.

2.2. Effective Potentials in Liquids. An effective potential u_{eff}, reproducing some property X of a system with potential u, is usually defined by requiring that the system with u_{eff} has the same value of the property as the system of interest,[5,6]

$$X(\rho,T;u_{eff}) = X(\rho,T;u) \tag{9}$$

In general, u_{eff} will be state and property dependent; that is, u_{eff} will change when reproducing different properties X of the same system.

In this work, we consider spherical effective potentials $u_{eff}(r)$ to reproduce the pressure ($X = p$) of fluids in isotropic phases. Let $\mathbf{r}$ and Ω be the relative position and orientation of two particles, and $g(r,\Omega)$ the two-particle distribution function.

Application of the virial theorem

$$p = \rho kT\left(1 - \frac{\rho}{6}\int \mathrm{d}^3 r \int \mathrm{d}\Omega r \frac{\partial u}{\partial r} g(r,\Omega;u)\right) \qquad (10)$$

to the true and effective potentials in order to satisfy eq 9

$$p_{\mathrm{eff}}(\rho,T) = p(\rho,T) \qquad (11)$$

means that a sufficient condition on u_{eff} is

$$\frac{\partial u_{\mathrm{eff}}}{\partial r} g(r;u_{\mathrm{eff}}) = \frac{1}{4\pi}\int \mathrm{d}\Omega \frac{\partial u}{\partial r} g(r,\Omega;u) \qquad (12)$$

The dependence of $g(r;u_{\mathrm{eff}})$ on $u_{\mathrm{eff}}(r)$ demands an iterative method to solve eq 12 that requires a computational effort additional to that of calculating $g(r,\Omega;u)$ from the true potential (by integral equations or computer simulations). Although the extra iterative computations can be circumvented by using appropriate families of effective potentials, as will be discussed below, this difficulty makes it necessary to clarify the usefulness of the concept of effective potential.

Effective potentials are useful in two different ways. The first applies when the pair potential is well-known: calculating $g(r,\Omega;u)$ in a set of states allows us to obtain u_{eff} in those states. If u_{eff} is of simple enough form and depends smoothly on the state variables, one can then use it to calculate the thermodynamics in other states with less effort. As an instance of this use, we can mention the effective potentials derived to account for three-body effects of the Axilrod−Teller type.[6,7]

The second use of effective potentials is in the case of real fluids where precise knowledge of $u(\mathbf{r},\Omega)$ is largely unavailable but whose thermodynamic properties have been measured experimentally on some states. Here, an effective potential not only allows us to calculate the properties in states different from those measured but also gives partial insight about the molecular interactions. This situation has been exhibited by the ANC theory for real gases.[8,9]

An alternative route to solving eq 12 in order to find u_{eff} that does not rely on computationally expensive iterations is to introduce a parametrized family of potentials with known EOS and then solving eq 11 for the potential parameters. In general, for a given family of u_{eff}, the potential thus found will solve eq 11 only approximately, although the definition of u_{eff} can be improved by inclusion of new parameters in order to obtain successively better approximations. The ANC theory for gases uses precisely this approach taking $u_{\mathrm{eff}}(r)$ as the ANC family of potentials, $u_s(r)$, eq 3. In this sense, the ANC potentials are "approximate effective potentials" for the nonconformal fluids they represent.

If eq 11 were solved exactly, one would get a mapping of the EOS of the fluid of interest onto the EOS of the parametrized family. This method has been used previously for spherical pair potentials using as effective interactions square wells of variable range,[10] but because these have a non realistic flat bottom, the effective parameters were found to vary strongly with the state.

The potentials $u_{\mathrm{eff}}(r)$ are state-dependent quantities because in calculating the average in eq 12 the ρ and T dependencies of $g(r,\Omega;u)$ and $g(r,u_{\mathrm{eff}})$ cancel only approximately. Therefore, when using a family as the ANC, parametrized by ϵ, r_{m}, and s, the potential parameters will also be state dependent. In particular, we expect that their finite density values will differ from their dilute gas limits. For hard bodies, the effective diameters for the pressure are influenced by changes in density, because the anisotropy of the particles promotes orientational correlations at high densities.[11] For soft molecules, we also expect a dependency of the parameters with the temperature.

3. Monte Carlo Simulation of ANC Fluids

To test the ANC theory's ability for supplying effective potentials of dense fluids, we needed data on the pressure of ANC fluids and a reliable EOS. With this purpose, we performed NVT Monte Carlo simulations of dense ANC fluids for three values of the softness: $s = 0.5$, 0.7, and 1.0. Simulations of the reference system were the most extensive (111 states), with 26 states for the $s = 0.7$ system and 5 states for $s = 0.5$.

The cubic simulation box contained 500 particles with a cutoff radius equal to half the width of the box. At given ρ^* and T^*, we calculated $g(r)$ and the reduced internal energy per particle, $U/N\epsilon$, as averages over configurations. Each run consisted of 4×10^7configurations; the first 10^7 were disregarded for equilibration purposes, and only the last 3×10^7 were used for averaging.

The reference was simulated at twelve isochores ($\rho^* = 0.1$, 0.2, 0.3, ..., and 1.2) and eight temperatures ($T^* = 0.8$, 1, 1.2, 1.5, 2, 3, 5, and 10), states referred to as the main grid. For $s = 0.7$ we used five isochores ($\rho^* = 0.5$, 0.7, 0.8, 1, and 1.2). Only one isochore, $\rho^* = 1$, was considered for $s = 0.5$. The simulations for the last system were not used to develop the ANC EOS but served as part of its test.

For each isochore, we started with a simulation at $T^* = 10$ from a fcc lattice. The next simulations were performed at successively lower temperatures, starting each time from the last previous configuration. Some of the cooler states on the main grid for $s = 1$ may be in the two-phase region and were not simulated.[12] A further 20 single-phase states were added near the saturation curve to enhance sampling in this part of the phase diagram. These states will be referred to as near-orthobaric states.

We calculated p^* by means of the virial theorem, eq 10, and included a tail correction with $g(r) = 1$ for r greater than the cutoff. The virial theorem was separated to get the repulsive and attractive contributions to the pressure (p_{R}^* and p_{A}^*, respectively). The rms standard deviation in p^* for the simulations with $s = 1$ was 0.5% and its maximum 3%.

The MC results are used below to develop an EOS for the ANC family and to assess its accuracy. Tables of results from the simulations are available via the Internet.[14]

4. Equation of State of ANC Fluids

Even though the straight results from the MC simulations can be used to analyze the variation of the properties with s, to apply the ANC theory, it is necessary to develop closed expressions for those properties, i.e., explicit equations of state. Several routes are available to this end: perturbation theories, empirical EOS, and collision properties mapping.[10] In this work, we concentrate on the first two routes (WCA and Song−Mason theories and a modified Benedict−Webb−Rubin equation) and discuss each EOS in turn.

4.1. WCA Perturbation Theory. Following the perturbative scheme proposed by WCA we divide $u_s(r)$ in its repulsive, u_{R}, and attractive, u_{A}, parts[15]

$$u_{\mathrm{R}}(r) = \begin{cases} u(r) + \epsilon & r \le r_{\mathrm{m}} \\ 0 & r > r_{\mathrm{m}} \end{cases}$$

$$u_{\mathrm{A}}(r) = \begin{cases} -\epsilon & r \le r_{\mathrm{m}} \\ u(r) & r > r_{\mathrm{m}} \end{cases}$$

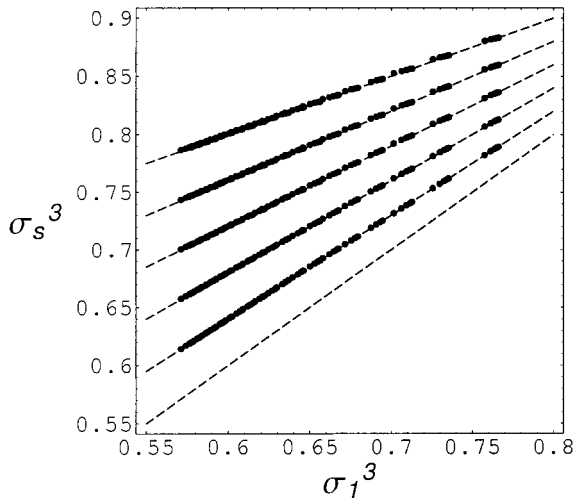

Figure 2. The function $\sigma_s^3(\sigma_1^3) = 1 + s(\sigma_1^3 - 1)$ for $s = 0.5, 0.6, ...,$ and 1 compared with direct evaluation of the WCA diameter σ_s (dots), for $0.1 \leq \rho^* \leq 1.2$ and $1 \leq T^* \leq 10$.

To calculate the properties of the unperturbed system, u_R, the theory considers a further perturbative expansion from a hard sphere (HS) system of suitable diameter d. To first order, the free energy of the unperturbed system becomes equal to that of the HS system

$$\beta a_R = \beta a_{HS}(\eta) \tag{13}$$

where $\eta = \pi\rho^*\sigma_s^3(\rho^*,T^*)/6$, $\sigma_s = d_s/r_m$, and d_s is chosen so that

$$\int_0^\infty dr\, r^2 y_{HS}(r/d_s)(\exp[-\beta u_R(r;s)] - \exp[-\beta u_{HS}(r;d_s)]) = 0 \tag{14}$$

We used the Grundke−Henderson parametrization to represent $y_{HS}(x)$.[16]

Because accurate closed form expressions for $\beta a_{HS}(\eta)$ are well-known, eq 13 provides an approximate EOS for $u_R(r)$ once d_s obtained from eq 14 is expressed as a function of ρ^* and T^*.

It is straightforward to prove from eq 14 that $\lim_{\rho^*\to 0}\sigma_s^3(\rho^*,T^*) = b_s^*(T^*)$. Because of this fact and eq 6, we tested at higher densities the linear relationship

$$\sigma_s^3 = 1 - s + s\sigma_1^3 \tag{15}$$

Figure 2 shows σ_s^3 calculated directly from eq 14 against σ_1^3 for $s = (0.5, 0.6, ...,$ and 1), compared with eq 15. A very good agreement is observed for all of the values of $\rho^*$and T^* tested ($0.1 \leq \rho^* \leq 1.2$ and $1 \leq T^* \leq 10$).

Another linear relationship, which makes the EOS fully explicit, was found between σ_1^3 and $b_1^*(T^*)$, namely

$$\sigma_1^3 = b_1^*(T^*) - 0.007\,864\rho^*$$

So that, σ_s^3 is fully known in terms of ρ^*, T^*, and s. Finally, the pressure is obtained from eq 13

$$p_R^* = \rho^* T^* z_{HS}(\eta)\left(1 + \frac{1}{\sigma_s^3}\frac{\partial \sigma_s^3}{\partial \rho^*}\right)$$

For $z_{HS}(\eta)$ we use the Carnahan−Starling HS compressibility factor

$$z_{HS}(\eta) = 4\eta y_{HS}^{\sigma}(\eta)$$

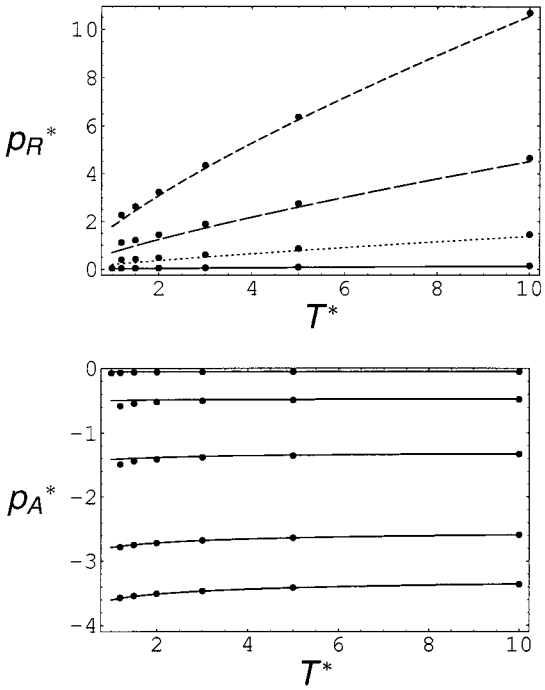

Figure 3. WCA repulsive and attractive pressures for the ANC reference (lines) compared with Monte Carlo simulation results reported in this work (circles).

where

$$y_{HS}^{\sigma}(\eta) = \frac{1 - \eta/2}{(1-\eta)^3}$$

represents the contact value of $y_{HS}(x)$.

The WCA perturbation theory does not incorporate explicitly the effects of the attractive forces. To complete the EOS, p_A^* was obtained numerically by the virial theorem using $y(r) = y_{HS}(r/d)$.

In Figure 3, we compare the WCA predictions of p_R^* and p_A^* for $u_1(r)$ with the MC results, showing that the prediction is very good at high T^* or ρ^* but with larger deviations at low T^* or ρ^* because in the latter conditions the attractive forces affect more the fluid structure. This effect is seen by comparison of the WCA with the MC $g(r)$, shown in Figure 4 with $s = 1$ at $T^* = 10$ for two densities, $\rho^* = 0.1$ and 0.4. The WCA approximation deteriorates as the density diminishes, mainly by underestimating the height of the peak of the simulated $g(r)$. This effect is more severe at lower T^*.

To summarize, WCA theory gives a total pressure that is only very accurate at high ρ and T. Nevertheless, the theory provides qualitative information about the effect of nonconformality for the ANC potentials, particularly about the dependence of the effective HS diameter on s.

4.2. Song−Mason (SM) Theory. A variant of perturbation theory that includes the effect of attractive forces in an explicit although approximate way is that of Song−Mason (SM).[17] It leads to the equation of state

$$\frac{\beta p}{\rho} = 1 + B(T)\rho + I(\rho,T)\rho$$

with

$$I(\rho,T) = \alpha(T)y_{HS}^{\sigma}(\eta) - 1$$

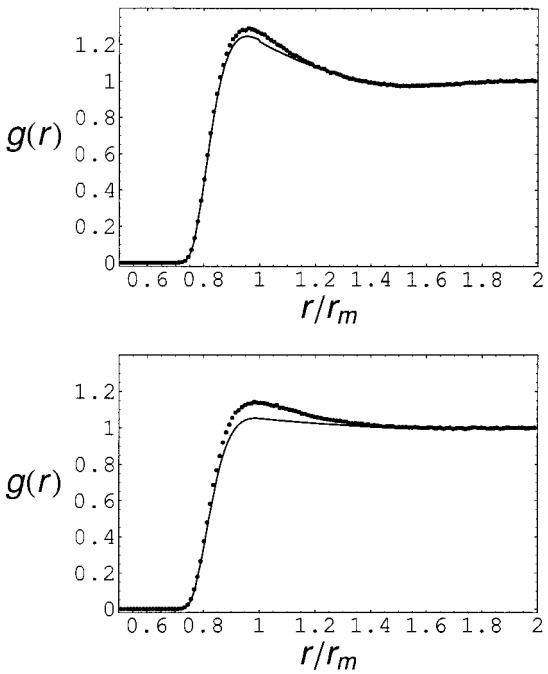

Figure 4. Comparison of WCA and MC $g(r)$ for the ANC reference (solid lines and dots) at $T^* = 10$ for two densities: $\rho^* = 0.4$ and $\rho^* = 0.1$ (upper and lower panels, respectively).

TABLE 1: ANC Critical Points from the Song−Mason EOS

s	ρ_c^*	T_c^*	p_c^*
0.5	0.408	0.744	0.109
0.7	0.382	0.903	0.123
1.0	0.350	1.111	0.139
1.2	0.333	1.235	0.147

where it can be shown that

$$\alpha(T) = \frac{2}{3}\pi {r_m}^3 b^*_s(T^*) \tag{16}$$

and

$$\eta = \frac{\rho}{4}\left(\alpha + T\frac{\partial \alpha}{\partial T}\right)$$

For ANC potentials and from eqs 6, 8, and 16 the SM functions $B(T)$ and $\alpha(T)$ are related linearly by s to those of the reference system.

The SM-EOS fares a little better than WCA theory when compared with the simulated data (it yields a rms relative error of 34% on the main grid states and 10% when only states with $T^* \geq 1.5$ are considered), but it incorporates into the EOS the contribution of the attractive forces in a closed form. This feature simplifies studying the dependency of the critical constants with the softness of the potential and gives a qualitatively correct picture of the vapor−liquid equilibria curves of ANC fluids.[12] The SM EOS predicts that softer potentials will have higher critical temperatures and pressures, and lower critical densities, than the harder ones do (see Table 1).

At any rate, the description of ANC systems with EOS obtained by perturbation theories, although illuminates the effect of varying s on the pressure, is not sufficiently precise to be used in testing the applicability of the ANC theory in dense fluids. However, the closed form of SM-EOS for ANC fluids may be advantageous for applications that do not demand high accuracy.

TABLE 2: Parameters for the ANC Reference EOS

m	k_m	m	k_m	m	k_m	m	k_m
1	0.94573	5	-0.37349	9	−9.50946	13	−1.87642
2	−1.21988	6	0.63383	10	19.47130	14	2.71703
3	−4.05036	7	0.93327	11	−8.73418	15	2.20851
4	1.57206	8	0.63005	12	−4.76513	16	0.64007

4.3. An Empirical EOS for ANC Fluids. To obtain the needed representation of the thermodynamics of ANC fluids, we developed an interpolative EOS for the ANC family. The situation is similar in part to the case of the Lennard-Jones fluid that is used as a reference in many studies and whose EOS has been obtained by fitting computer simulation results. Nevertheless, in our case, we need not only an EOS for the ANC reference fluid but also for the family of nonconformal fluids. In this section, we describe how the reference EOS was obtained and how the simulated $g(r)$ for values of s were employed to extend the EOS to other ANC fluids.

The desired reference EOS was found by choosing an empirical functional form for $p_1^*(\rho^*,T^*)$ and fitting its coefficients by least squares over all main grid and near-orthobaric states. Because subcritical states had a smaller weight than supercritical ones, the resulting EOS is expected to work better in supercritical conditions. Further, because the ANC theory gives very good results in the gas-phase we imposed the correct low-density limit to the desired EOS.

Among the several empirical EOS tried (Peng−Robinson, Redlich−Kwong, and Benedict−Webb−Rubin), the best functional form was found to be the modified BWR equation used for the IUPAC tables of argon[18]

$$p_1^*(\rho^*,T^*) = \rho^*T^*\left(1 + \rho^*\sum_{m=1}^{5}\frac{k_m}{T^{*m-1}} + \rho^{*2}\left(k_6 + \frac{k_7}{T^*}\right) + \rho^{*3}k_8 + \rho^{*5}\frac{k_{15}}{T^*} + \rho^{*2}\left(\sum_{m=9}^{11}\frac{k_m}{T^{*m-6}} + \rho^{*2}\sum_{m=12}^{14}\frac{k_m}{T^{*m-9}}\right)\exp(-k_{16}\rho^{*2})\right) \tag{17}$$

It is important to note that the terms from k_1 through k_5 give $B_1^*(T^*)$. Following the fitting procedure of Johnson et al. for the Lennard-Jones fluid,[19] we fitted these five coefficients to $B_1^*(T^*)$ data calculated directly and kept them fixed through the fitting of the rest of the k_i. The values so obtained are reported in Table 2. Equation 17 requires 16 parameters, whereas the LJ EOS of Johnson et al. uses 33 parameters; this reduction is due to the fact that the weight of subcritical MC states is lower.

Equation 17 represents the main grid states with a rms relative error of 1.3% and of 3.1% when the near-orthobaric states are also considered. This degree of precision is an order of magnitude better than in the perturbation theory EOS and was considered sufficient in order to test and apply the ANC theory.

To obtain the thermodynamics for $s \neq 1$, we considered the free energy of the fluid as a function of ρ, T, and s on an equal footing:[20,21]

$$dA = -SdT - pdV - Lds$$

The thermodynamic definition of L is

$$L \equiv -\frac{\partial A}{\partial s} = kT\frac{\partial}{\partial s}\ln Q$$

Because the ideal partition function does not depend on the

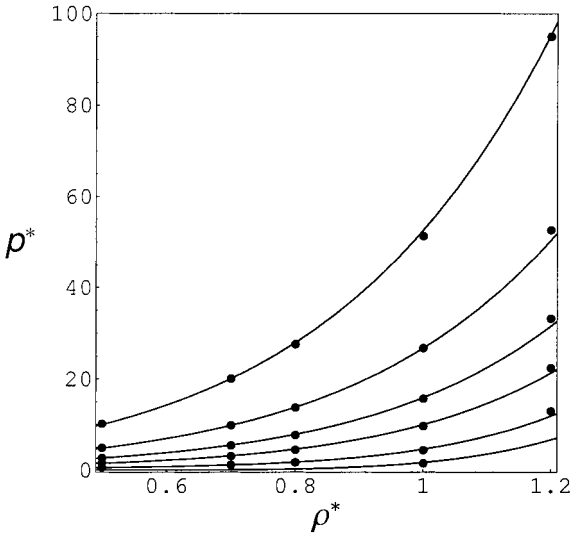

Figure 5. Isotherms of p^* for the ANC $s = 0.7$ system predicted by the ANC EOS, eq 20, compared with MC data (circles).

shape of the potential, L depends only on the configurational partition function

$$Q_N = \frac{1}{V^N}\int \mathrm{d}\{N\}\, \exp[-\beta U(\{N\})]$$

from which one finds

$$L = \frac{kT}{Q_N}\frac{\partial Q_N}{\partial s}$$

Defining $l = L/N\epsilon$, one obtains

$$l(\rho^*,T^*,s) = -2\pi\rho^* \int_0^\infty z^2 \frac{\partial u_s^*(z)}{\partial s}\, g(z)\, \mathrm{d}z \qquad (18)$$

which allows us to calculate l from simulated results of $g(z)$. Finally, a Maxwell relation enables us to calculate the variation of pressure as the softness of the potential changes

$$\frac{\partial p^*}{\partial s} = -\rho^{*2}\frac{\partial l}{\partial \rho^*} \qquad (19)$$

The problem of constructing EOS for the ANC family is reduced to calculating l by eq 18 for given values of s, followed by integration of eq 19. Because calculation of l requires extensive simulations for each value of s we used Lagrange interpolation: l was calculated at all simulated states for $s_1 = 1$ and $s_2 = 0.7$, the results fitted with a polynomial in ρ^* and $1/T^*$ to obtain a first-order interpolation

$$l_s(\rho^*,T^*) = \frac{10}{3}[(s-0.7)l_1(\rho^*,\mathrm{T}^*) - (s-1)l_{0.7}(\rho^*,\mathrm{T}^*)]$$

Details of $l_{0.7}$ and l_1 are given in the Appendix.

The above procedure leads to the desired EOS for the ANC family with a single softness

$$p^*(\rho^*,T^*,s) = p_1^*(\rho^*,T^*) - \frac{1}{2}(s-1)\rho^{*2}\frac{\partial}{\partial\rho^*}[l_1(\rho^*,T^*) + l_s(\rho^*,T^*)] \qquad (20)$$

which means that p^* is a quadratic function of s.

As a test of this ANC EOS, we used it to calculate p^* at the simulated states for $s = 0.7$. We note that only simulated $g(r)$ data for this system, and not the pressures, were used to develop eq 20. Figure 5 shows good agreement of eq 20 with the MC data, with a rms relative error around 3% which is of the same order as that of the reference EOS. A further test was made for $s = 0.5$ using the MC supercritical data. A rms error of 5% was found at the $\rho^* = 1$ isochore with $T^* = 1.2$, 2, 3, and 5. Because most fluids studied in the gas phase have $0.5 < s < 1.2$, this EOS should be useful in many applications.

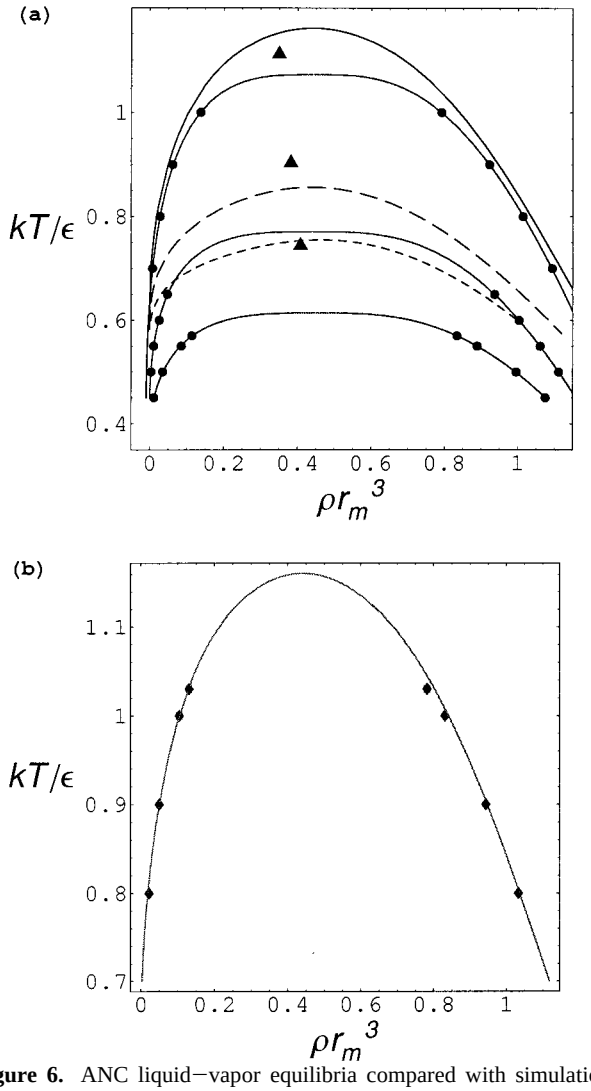

Figure 6. ANC liquid−vapor equilibria compared with simulation results (a) comparison of ANC EOS saturation curves for $s = 0.5$, 0.7, and 1 (from bottom to top, with symbols as in Figure 1) compared with extrapolated MD simulation results (circles). Song−Mason critical points are shown as triangles. (b) ANC EOS saturation curve for $s = 1$ compared with GEMC simulation results.

It must be granted that the empirical eqs 17 and 20 have many parameters and that they need improvement in subcritical states. Nevertheless, it should be pointed out that according to the ANC theory these equations are constructed only once but will be applied to many nonconformal fluids.

Although at this stage of the present work we have obtained an ANC EOS useful in supercritical conditions, it is interesting to see how the two-phase behavior changes with s. Figure 6a compares the saturation curves of eq 20 with those recently obtained by direct MD simulation of the liquid−vapor equilibria of the ANC fluids and extrapolated to the critical region assuming universal exponents.[12] The MD curves are flatter and with lower T_c^* than those of eq 20. This may be due at least in part to the fact that eq 20 has classical critical exponents and that the MD extrapolations used universal exponents. Further,

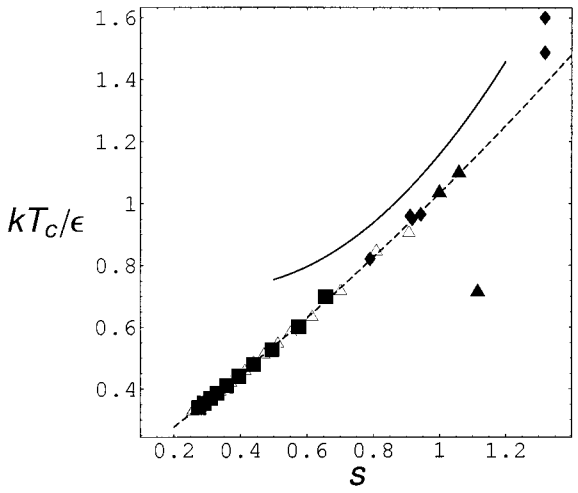

Figure 7. Reduced critical temperature as a function of s, from the inversion of $B(T)$ for real fluids (dashed line) compared with the ANC EOS prediction (solid line). The three right-most points correspond to He, H_2, and D_2 (from left to right).

the MD simulations truncated and shifted the potentials, so that the resulting T_c^* are lower than the exact ones.[22] New simulations were deemed necessary to settle this point.

Very recently, Ramos and del Río have obtained a new estimation of the saturation curve of untruncated ANC systems via Gibbs ensemble Monte Carlo methods.[13] Figure 6b compares the GEMC results for $s = 1$ with the curve predicted by eq 20. Excelent agreement is found up to the highest simulated temperature, although we expect that at temperatures closer to the critical eq 20 will eventually fail to give the universal behavior.

The ANC EOS, eq 20, predicts that T_c^* diminishes with s (see Figure 7) in qualitative agreement with the T_c^* against s correlation found in the low-density limit. The discrepancy can be due to the lack of precision of eq 20 at subcritical temperatures and to the fact that real substances will have effective parameters at the critical density different from those in the dilute gas.

5. Application to Model Fluids

We applied the ANC theory to model systems on single phase states where eq 20 represents well the pressure of ANC systems. To do so, for each system of interest, we determined ϵ, r_m, and s which satisfy approximately eq 11 over the sets of states on which the right-hand side of this equation has been evaluated by simulation. For several of the fluids here considered, some of the effective parameters are state dependent, and hence, models for this dependence have to be introduced. These models take into account two sources of nonconformality: the profile of the pair potential functions and the shape of the molecules examined. The fluids considered in this section were chosen because they incorporate both effects.

We study first as a simple spherical interaction the 12−6 Lennard-Jones potential[19] and then turn to nonspherical systems. These are Kihara spherocylinders, which have constant depth for all orientations and a nonspherical hard core,[23] two-center Lennard-Jones diatomics, with orientationally dependent depths and homonuclear hard cores,[24] and finally, heteronuclear diatomics made of bonded square-wells.[25]

5.1. Lennard-Jones Fluid. The classic Lennard-Jones potential is given by

$$u_{LJ}(r) = 4\epsilon_{LJ}\left(\left(\frac{\sigma}{r}\right)^{12} - \left(\frac{\sigma}{r}\right)^{6}\right)$$

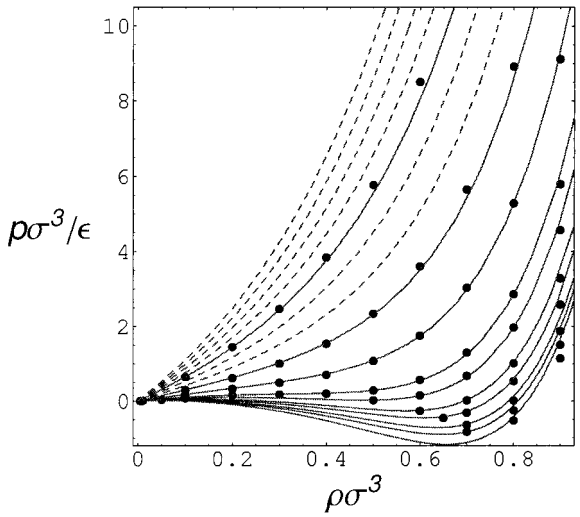

Figure 8. ANC isotherms of the pressure for the Lennard-Jones fluid compared with Johnson et al. MC data. Dashed isotherms correspond to temperatures not simulated.

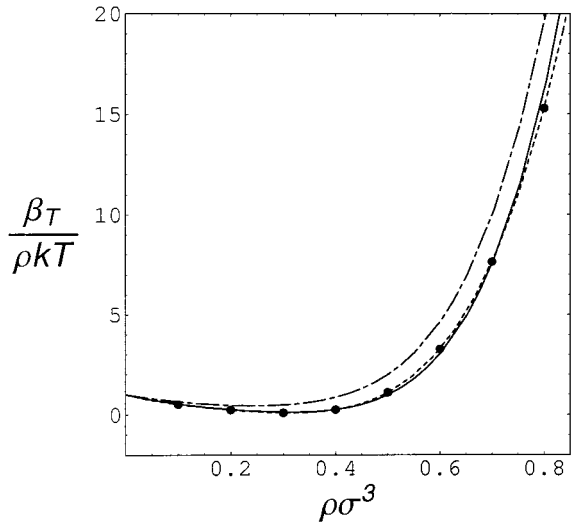

Figure 9. ANC reduced coefficient of isothermal compressibility, $\beta_T/\rho kT$, for the LJ fluid at $T^* = 1.4$ (solid line) compared with results from interpolation of Johnson et al. MC data (circles and dashed line). The same isotherm for the ANC reference (long−short-dashed line) illustrates the dependence with s.

Being spherical, the LJ nonconformality with $u_1(r)$ is entirely due to the form of its profile. As a first trial, we assumed effective parameters constant and equal to their low-density limits $\epsilon = \epsilon_{LJ}$, $r_m = 2^{1/6}\sigma$, and $s = 1.126\,27$. In Figure 8, we compare the ANC EOS predicted pressure with the simulation results of Johnson et al.[19] The agreement is good at high temperatures for all densities (with an rms error of 5% for all states with $T^* \geq 1.2$). Not surprisingly, because of the inaccuracy of the ANC reference EOS at subcritical temperatures, the prediction at $T^* = 0.8$ is rather poor.

To see another effect of the softness s, we compared the isothermal coefficient of bulk compressibility, $\beta_T = \kappa_T^{-1}$, from the ANC EOS with that obtained from interpolation of the Johnson et al. data. Figure 9 shows good agreement between the two results (again, at supercritical temperatures). In the same figure, we can see that $\beta_T(s = 1) > \beta_T(\mathrm{LJ})$ at every density, because the latter's greater value of s implies a greater compressibility. It is clear that the ANC effective potential with the same parameters as those in the dilute gas represents well the Lennard-Jones EOS at high densities. A similar degree of

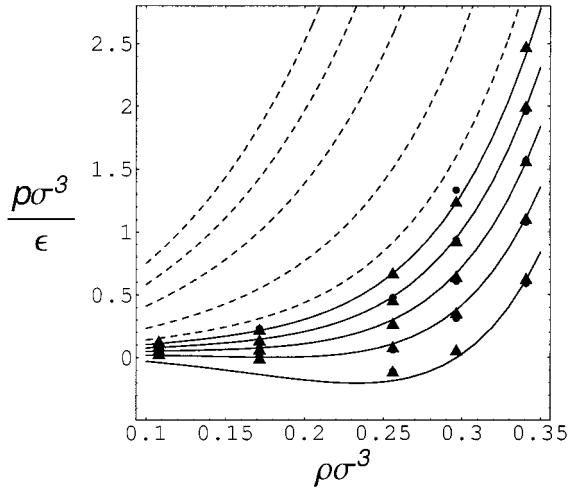

Figure 10. ANC isotherms of the pressure for Kihara spherocylinders with $l^* = 1$. MC and "improved perturbation theory" results from Vega et al. are shown for comparison (circles and triangles, respectively). Dashed isotherms as in Figure 8.

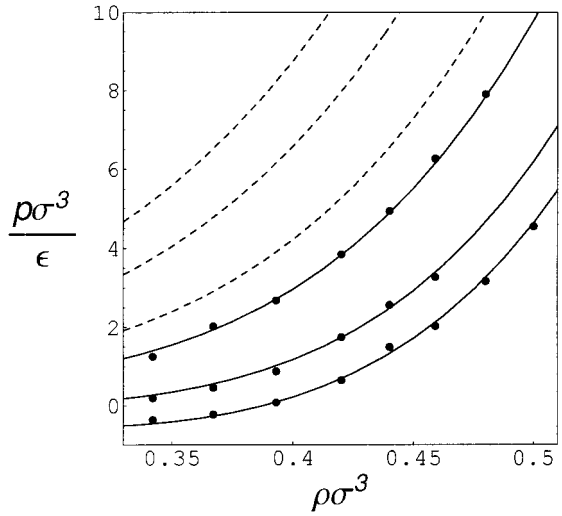

Figure 11. ANC isotherms of the pressure for two-center Lennard-Jones with $l^* = 0.793$ compared with simulation data from Lombardero et al. Dashed isotherms as in Figure 8.

precision can be expected of the ANC predictions for other spherical interactions with $0.5 < s < 1.2$. (Although, of course, the ANC EOS needs improvement in the subcritical region.)

5.2. Kihara Spherocylinders. This potential is defined for molecules with spherocylindrical hard cores of width σ and distance between the sphere centers d, its elongation is defined as $l^* = d/\sigma$. The functional form is

$$u_{\mathrm{KSC}}(\mathbf{r},\Omega) = 4\epsilon_{\mathrm{KSC}}\left(\left(\frac{\sigma}{R(\mathbf{r},\Omega)}\right)^{12} - \left(\frac{\sigma}{R(\mathbf{r},\Omega)}\right)^{6}\right)$$

where $R(\mathbf{r},\Omega)$ is the shortest distance between the hard cores. For this test, we selected the system with $l^* = 1$ which has been studied by simulations.

Because the depth of the potential is independent of orientations we expect ϵ to remain constant, and thus, we take $\epsilon = \epsilon_{\mathrm{KSC}}$ as the effective depth. Ramos et al. studied the linear Kihara gas in a two-softness approximation with different values for the repulsive and attractive parts of the potential. In a perturbation theory spirit, we have simply set s equal to the repulsive softness at low densities $s = 0.7944$.[4]

Because the system is nonspherical, we expect the effective diameter to diminish with increasing density because the spherocylinders tend to align.[11] To represent this behavior, we propose a virial-like series starting from the zero density value $r_{\mathrm{m}}^{(0)} = 1.5961$ obtained by Ramos et al.[4]

$$r_{\mathrm{m}}/\sigma = r_{\mathrm{m}}^{(0)} + r_{\mathrm{m}}^{(1)}\rho\sigma^3 + r_{\mathrm{m}}^{(2)}(\rho\sigma^3)^2$$

The other coefficients were obtained by least squares solution of eq 11 for the simulations results of Vega et al.,[23] obtaining $r_{\mathrm{m}}^{(1)} = -0.561$ and $r_{\mathrm{m}}^{(2)} = 0.76$. This makes r_{m} a monotonic decreasing function of ρ in the simulated range, as it should. Figure 10 compares the results of Vega et al. MC simulations and of their "improved perturbation theory" with the ANC results. The agreement is good with the exception of the $T^* = 0.7$ isotherm. In the same figure, plots of other isotherms predicted by the ANC model are shown.

5.3. Two-Center Lennard-Jones. The two-center Lennard-Jones potential models a diatomic by two interaction sites located at the "atomic" centers. The energy of two particles is obtained as the sum of spherical Lennard-Jones potentials of the inter-site distances. Let $\mathbf{r}_{i\mu}$ be the position of the μth site in the ith molecule, then the potential between particles **1** and **2** is

$$u_{2\mathrm{LJ}}(\mathbf{1},\mathbf{2}) = \sum_{\mu=1}^{2}\sum_{\nu=1}^{2} u_{\mathrm{LJ}}(|\mathbf{r}_{1\mu} - \mathbf{r}_{2\nu}|)$$

The distance between the sites in a particle is d, and the molecular elongation is $l^* = d/\sigma$. As a test, we consider here the case with $l^* = 0.793$. The ANC inversion of $B(T)$ for two-center Lennard-Jones provides us with values for the low-density limit of the ANC parameters: $\epsilon^{(0)}/\epsilon_{\mathrm{LJ}} = 2.324\,09$, $r_{\mathrm{m}}^{(0)}/\sigma = 1.36542$, $s^{(0)} = 0.7960$.[4]

As before, we expect the molecules to align when ρ increases, leading to a decrease in r_{m}. Nevertheless, alignment will also hinder the opportunities for the sites getting close enough to contribute with the maximum depth $4\epsilon_{\mathrm{LJ}}$ to the potential, and hence, one would also expect ϵ to decrease. Keeping the softness constant, $s = s^{(0)}$, we used the following model for ϵ and r_{m} to find a least-squares solution of eq 11 for the results of Lombardero et al.:[24]

$$\epsilon/\epsilon_{\mathrm{LJ}} = \epsilon^{(0)} + \epsilon^{(1)}\rho\sigma^3$$

$$r_{\mathrm{m}}/\sigma = r_{\mathrm{m}}^{(0)} + r_{\mathrm{m}}^{(1)}\rho\sigma^3$$

We obtained $\epsilon^{(1)} = -0.631$ and $r_{\mathrm{m}}^{(1)} = -0.0260$, negative as expected. Figure 11 compares the ANC and simulated results for the pressure. The agreement is good for the three isotherms $kT/\epsilon_{\mathrm{LJ}} = (1.5, 1.8, 2.5)$. The same figure shows the ANC prediction for the pressure at other temperatures.

5.4. Bonded Square Wells. Finally, we turn to an heteronuclear diatomic modeled by a discontinuous potential, the bonded square well (BSW). This potential has the form

$$u_{\mathrm{BSW}}(\mathbf{1},\mathbf{2}) = \sum_{\mu=1}^{2}\sum_{\nu=1}^{2} u_{\mu\nu}(|\mathbf{r}_{1\mu} - \mathbf{r}_{2\nu}|)$$

where $u_{\mu\nu}(r)$ are square well potentials

$$u_{\mu\nu}(r) = \begin{cases} \infty & r < \sigma_{\mu\nu} \\ -\epsilon_{\mu\nu} & \sigma_{\mu\nu} \le r \le \lambda_{\mu\nu}\sigma_{\mu\nu} \\ 0 & r > \lambda_{\mu\nu}\sigma_{\mu\nu} \end{cases}$$

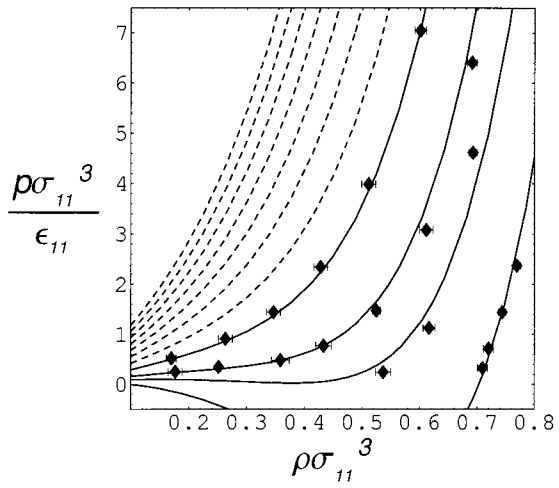

Figure 12. ANC isotherms of the pressure for the bonded square well system I of McCabe et al. compared with MC data. Dashed isotherms as in Figure 8.

Because the hard cores of the square wells are tangent, the potential is fully described by providing three symmetric matrices whose elements are $\epsilon_{\mu\nu}$, $\sigma_{\mu\nu}$, and $\lambda_{\mu\nu}$. In this work, we will discuss the representation of the first BSW system simulated by McCabe et al.[25] The system is heteronuclear, with

$$\epsilon_{22} = \epsilon_{12} = \epsilon_{11}$$

$$\sigma_{22} = \sigma_{11}/2, \quad \sigma_{12} = 3\sigma_{11}/4$$

$$\lambda_{22} = \lambda_{12} = \lambda_{11} = 3/2$$

The low-density limit of the ANC parameters for this system can be calculated by inverting $B(T)$ from the SAFT-VR equation of state.[25] Nevertheless, this equation is not exact, and hence, the parameters obtained from it were not useful to evaluate the effective potential at zero density, except for the softness $s^{(0)} = 0.906$. Hence, the fitting procedure to determine the state dependency of the effective parameters did not fix the zero density values of ϵ and r_m. The final model used was

$$\epsilon/\epsilon_{11} = \epsilon^{(0)}$$

$$r_m/\sigma_{11} = r_m^{(0)} + r_m^{(1)}\epsilon_{11}/kT$$

$$s = s^{(0)}$$

From the McCabe et al. simulation data we found $\epsilon^{(0)} = 1.577$, $r_m^{(0)} = 1.2208$, and $r_m^{(1)} = -0.0487$. Figure 12 presents the ANC results compared to the simulation data, the agreement is good for three isotherms, whereas for $kT/\epsilon_{11} = 1.5$, it is less satisfactory. It is interesting to notice that r_m increases with T, whereas its ρ dependence is not apparent.

6. Conclusions

We have shown that the ANC theory provides closed form EOS for dense fluids which are in good agreement with simulation results and that allow us to predict the pressure at supercritical states. Furthermore, the ANC family of nonconformal potentials appears to be useful to represent effective interactions in model dense fluids.

For the LJ spherical system tested, the effective potential was found to be state independent. For the nonspherical systems, the state dependency of the effective potentials is reflected on a slight although important dependence of ϵ and r_m on ρ and T, whereas the shape parameter s remains constant.

Because of the similarity of ANC potentials and realistic systems, the state dependency of the effective parameters is greatly simplified compared to that of variable range square wells.[10]

Several improvements and extensions of ANC theory are in order: First, many-body forces must be included in order to apply it to real dense fluids; this will be the subject of a forthcoming paper. Second, the underlying ANC EOS must be revisited in subcritical conditions if phase equilibria are to be considered.

Acknowledgment. O. G. acknowledges funding from CONACYT for graduate study and a Mexican Institute of Petroleum (IMP) Ph.D. thesis scholarship and thanks Dr. José Alejandre for his supervision at IMP.

Appendix

Analysis of $B^*(T^*)$ for ANC systems provides the low-density limit of l

$$l^{(0)} = \frac{2}{3}\pi(1 - B_1^*(T^*))\rho^*T^*$$

For dense states, l was numerically calculated from eq 18 using the simulated $g(r)$ and the difference $l - l^{(0)}$ was fitted with a polynomial in ρ^* and $1/T^*$, so that

$$l_s(\rho^*,T^*) = l^{(0)} + (\rho^*T^*)^2\sum_{m=1}^{3}\sum_{n=1}^{4}\rho^{*m}\mathscr{M}(s)_{mn}(1/T^*)^n$$

where the matrices $\mathscr{M}(s)$ for $s = 1$ and $s = 0.7$ are

$$\mathscr{M}(1) = \begin{pmatrix} 2.6644 & -3.8682 & -2.7346 & 0 \\ -1.8767 & 4.0818 & 1.3950 & 0 \\ 0.40122 & 0.23051 & -1.6870 & 0.79046 \end{pmatrix}$$

$$\mathscr{M}(0.7) = \begin{pmatrix} 3.1430 & -0.9996 & -4.6500 & 0 \\ -1.7789 & -1.4493 & 5.3935 & 0 \\ 0.66967 & 1.0320 & -1.0458 & -0.36585 \end{pmatrix}$$

References and Notes

(1) Rowlinson, J. S.; Swinton, F. L. *Liquids and Liquid Mixtures*, 3rd ed.; Butterworth: London, 1982; Chapter 7.
(2) Pitzer, K. S.; Curl, R. J. *J. Am. Chem. Soc.* **1957**, *79*, 2369.
(3) del Río, F.; Ramos, J. E.; McLure, I. A. *J. Phys. Chem. B* **1998**, *102*, 10568.
(4) Ramos, J. E.; del Río, F.; McLure, I. A. *J. Phys. Chem. B* **1998**, *102*, 10576.
(5) Casanova, G.; Dulla, R. J.; Jonah, D. A.; Rowlinson, J. S.; Saville, G. *Mol. Phys.* **1970**, *18*, 589.
(6) van der Hoef, M. A.; Madden, P. A. *J. Chem. Phys.* **1999**, *111*, 1520.
(7) Attard, P. *Phys. Rev. A* **1992**, *45*, 3659.
(8) McLure, I. A.; Ramos, J. E.; del Río, F. *J. Phys. Chem. B* **1999**, *103*, 7019.
(9) del Río, F.; Ramos, J. E.; McLure, I. A. *Phys. Chem. Chem. Phys.* **1999**, *1*, 4937.
(10) Gil-Villegas, A.; del Río, F. *Phys. Rev. E* **1996**, *53*, 2326.
(11) del Río, F. *Mol. Phys.* **1981**, *42*, 217.
(12) del Río, F.; Ávalos, E.; Alejandre, J.; Díaz, E. To be published.
(13) Ramos, J. E.; del Río, F. Private communication.
(14) Department of Physics, UAM *Theoretical Molecular Thermodynamics*, http://fisica.uam.mx/english/research/liquidos/tmt.html.
(15) Hansen, J. P.; McDonald, I. R. *Theory of Simple Liquids*, 2nd ed.; Academic Press: London, 1986; Chapter 6.
(16) Henderson, D.; Grundke, E. W. *J. Chem. Phys.* **1975**, *63*, 601.

(17) Song, Y.; Mason, E. *J. Chem. Phys.* **1989**, *91*, 7840.
(18) *International Thermodynamic Tables of the Fluid State, Argon, 1971*; Angus, S., Armstrong, B., Ed.; Butterworth: London, 1972.
(19) Johnson, J. K.; Zollweg, J. A.; Gubbins, K. E. *Mol. Phys.* **1993**, *78*, 591.
(20) Landau, L.; Lifshitz, E. *Statistical Physics*, 3rd ed; Pergamon Press: Oxford, 1980; Chapter 2.
(21) Kofke, D. A. *Mol. Phys.* **1993**, *78*, 1331.
(22) Trokhymchuk, A.; Alejandre, J. *J. Chem. Phys.* **1999**, *111*, 8510.
(23) Vega, C.; Lago, S. *Chem. Phys. Lett.* **1991**, *185*, 516.
(24) Lombardero, M.; Martín, C.; Lomba, E. *J. Chem. Phys.* **1992**, *97*, 2724.
(25) McCabe, C.; Gil-Villegas, A.; Jackson, G.; del Río, F. *Mol. Phys.* **1999**, *97*, 551.